JGR Biogeosciences

RESEARCH ARTICLE
10.1029/2022JG006916

Special Section:
Advances in scaling and modeling of land-atmosphere interactions

Disentangling the Relative Drivers of Seasonal Evapotranspiration Across a Continental-Scale Aridity Gradient

Adam M. Young[1,2], Mark A. Friedl[3], Kimberly Novick[4], Russell L. Scott[5], Minkyu Moon[3], Steve Frolking[6], Xiaolu Li[7], Carlos M. Carrillo[7], and Andrew D. Richardson[1,2]

[1]Center for Ecosystem Science and Society, Northern Arizona University, Flagstaff, AZ, USA, [2]School of Informatics, Computing, and Cyber Systems, Northern Arizona University, Flagstaff, AZ, USA, [3]Department of Earth and Environment, Boston University, Boston, MA, USA, [4]O'Neill School of Public and Environmental Affairs, Indiana University, Bloomington, Bloomington, IN, USA, [5]Southwest Watershed Research Center, USDA-Agricultural Research Service, Tucson, AZ, USA, [6]Institute for the Study of Earth, Oceans, and Space, University of New Hampshire, Durham, NH, USA, [7]Department of Earth and Atmospheric Sciences, Cornell University, Ithaca, NY, USA

Key Points:

- In terrestrial ecosystems of North America, evapotranspiration (*ET*) displays strong seasonal patterns
- Path analysis was used to explore how the drivers of *ET* seasonality vary among different ecosystems and hydroclimate regimes
- Phenology emerged as the best predictor of *ET* in energy-limited regions; precipitation had a higher effect in water-limited ecosystems

Supporting Information:

Supporting Information may be found in the online version of this article.

Correspondence to:

A. M. Young,
adam.young@nau.edu

Citation:

Young, A. M., Friedl, M. A., Novick, K., Scott, R. L., Moon, M., Frolking, S., et al. (2022). Disentangling the relative drivers of seasonal evapotranspiration across a continental-scale aridity gradient. *Journal of Geophysical Research: Biogeosciences*, *127*, e2022JG006916. https://doi.org/10.1029/2022JG006916

Received 25 MAR 2022
Accepted 27 JUN 2022

© 2022. American Geophysical Union. All Rights Reserved.

Abstract Evapotranspiration (*ET*) is a significant ecosystem flux, governing the partitioning of energy at the land surface. Understanding the seasonal pattern and magnitude of *ET* is critical for anticipating a range of ecosystem impacts, including drought, heat-wave events, and plant mortality. In this study, we identified the relative controls of seasonal variability in *ET*, and how these controls vary among ecosystems. We used overlapping AmeriFlux and PhenoCam time series at a daily timestep from 20 sites to explore these linkages (# site-years >100), and our study area covered a broad climatological aridity gradient in the U.S. and Canada. We focused on disentangling the most important controls of bulk surface conductance (G_s) and evaporative fraction ($EF = LE/[H + LE]$), where *LE* and *H* represent latent and sensible heat fluxes, respectively. Specifically, we investigated how vegetation phenology varied in importance relative to meteorological variables (vapor pressure deficit and antecedent precipitation) as a driver of G_s and *EF* using path analysis, a framework for quantifying and comparing the causal linkages among multiple response and explanatory variables. Our results revealed that the drivers of G_s and *EF* seasonality varied significantly between energy- and water-limited ecosystems. Specifically, precipitation had a much higher effect in water-limited ecosystems, while seasonal patterns in canopy greenness emerged as a stronger control in energy-limited ecosystems. Given that phenology is expected to shift under future climate, our findings provide key information for understanding and predicting how phenology may impact 21st-century hydroclimate regimes and the surface-energy balance.

Plain Language Summary Surface-to-atmosphere water fluxes (i.e., evapotranspiration) are an important dynamic of terrestrial ecosystems, influencing the timing and severity of impacts such as drought, heat-wave events, and plant mortality. In this study, we explored why seasonal variability in evapotranspiration (*ET*) varies among a wide range of ecosystems. To conduct this work, we used AmeriFlux and PhenoCam datasets, which measure daily meteorological conditions and canopy greenness, respectively, from 20 individual sites. Our study area covered a broad climatological aridity gradient in the US and Canada, spanning from deciduous forests ecosystems in the northeast to drylands in the southwest. The most important finding from this work was that reoccurring patterns in vegetation green-up and senescence (i.e., phenology) consistently emerged as one of the strongest predictors of *ET* in ecosystems where water was non-limiting. By comparison, seasonal patterns in precipitation were identified as the strongest control of *ET* seasonality in dryland ecosystems where water is considerably scarcer, and phenology had much weaker influence in these regions. Overall, this study provides key insight into the sensitivity of *ET* seasonality to various drivers and ecosystem water availability.

1. Introduction

Evapotranspiration (*ET*) is a fundamental earth-system process that drives the water cycle, returning ~60% of precipitation over land to the atmosphere and exerting tight control over changes in land-surface temperature and surface energy balance (Oki & Kanae, 2006; Seneviratne et al., 2010; Wolf et al., 2016). *ET* displays strong seasonality in many terrestrial ecosystems, and inter-annual variation in the timing and magnitude in seasonal

shifts of *ET* can have considerable ecological and societal impacts. For example, early growing season anomalies of higher *ET* coincident with lower precipitation can lead to soil desiccation, warmer surface temperatures, and extreme heat-wave events later in year (Fischer et al., 2007; Lian et al., 2020; Miralles et al., 2014). Seasonal variability in the surface energy balance can affect land atmosphere coupling as well. For example, seasonal shifts in the Bowen ratio (*H*/*LE*)—driven by higher *ET*—can contribute to a shallower atmospheric boundary layer height and a higher likelihood of convective cloud formation (Konings et al., 2010; Manoli et al., 2016). Land-surface models also indicate that the land-surface energy balance is sensitive to seasonal anomalies in vegetation phenology and soil moisture (Fitzjarrald et al., 2001; Kim & Wang, 2007; Lu & Shuttleworth, 2002; Schär et al., 1999). Given expected shifts in hydroclimate under future climate change (Marvel et al., 2021), it is important to understand how the relative controls of seasonal *ET* vary among a wide range of ecosystems and under different hydrological regimes, particularly for predicting ecosystem water balance and drought.

Vegetation phenology has been consistently identified as a key control of seasonal variability of *ET* in some ecosystems (Baldocchi et al., 2010; Barr et al., 2007), and remote-sensing applications commonly use measures of vegetation seasonality to predict *ET* across broad spatial areas (Glenn et al., 2010). In temperate and boreal deciduous broadleaf forests, seasonal changes in leaf area index (LAI) are tightly coupled to changes in *ET*, highlighted by clear decreases in the Bowen ratio during leaf emergence (Blanken & Black, 2004; Schwartz, 1992; Wilson & Baldocchi, 2000). These linkages are a product of increased water loss via stomata during photosynthesis, and while seasonal changes and phenology of LAI are recognized as a key driver of *ET* in deciduous broadleaf forests, there has been less work evaluating these linkages across a broader range of plant functional types (PFTs) and among different hydrologic regimes (i.e., energy- vs. water-limited systems). As an example, in evergreen needleleaf forests, there are clear seasonal signals in photosynthetic activity and *ET* (Bowling et al., 2018; Seyednasrollah et al., 2021; Stoy et al., 2006), even though annual leaf turnover is considerably less compared to deciduous forests. However, it remains unclear how influential phenology is relative to other factors, particularly atmospheric and surface dryness represented by vapor pressure deficit (VPD) and precipitation, in evergreen needleleaf forests (e.g., Samuels-Crow et al., 2020; Stoy et al., 2006). The relative control of phenology compared to such meteorological factors remains uncertain in non-forested PFTs as well (e.g., Mackay et al., 2007; Moon et al., 2020). Given that phenological patterns are shifting in many terrestrial ecosystems, understanding how phenology acts as a key control of *ET* seasonality will help inform how water loss may evolve during the course of the growing season.

Understanding how the relative controls of *ET* vary among different ecosystems will also depend on climatological aridity, which defines whether *ET* is limited primarily by energy- or water-availability (Williams et al., 2012; Zhang et al., 2001). Variability in the primary drivers of *ET* during the growing season has been well identified in past studies. For example, during the growing season in energy-limited ecosystems with an ample water supply, VPD is likely to exert more influence over *ET* (Novick et al., 2016). Conversely, in water-limited ecosystems, including semi-arid and arid regions, precipitation and soil water content plays a much larger role in governing *ET* (Liu et al., 2020). At seasonal time scales, several studies have suggested seasonality in LAI can vary in importance as a control of *ET* (Guillevic et al., 2002; Han et al., 2020; Thompson et al., 2011). However, there remains little consensus regarding under what conditions or in which hydrologic regimes phenology acts as the dominant control of seasonal *ET*.

Increasing availability of high-resolution datasets (i.e., sub-daily to daily) of canopy plant activity and surface-atmosphere energy fluxes (e.g., *H* and *LE*) provide the key measurements needed to explore how the relative controls of *ET* vary at seasonal time scales. Specifically, evaluating such datasets would allow for identifying how closely *ET* tracks phenology and other key environmental variables at short time scales (e.g., days) and over multiple years. As a proof-of-concept, we evaluated time series for two AmeriFlux sites that generally span the continental-scale aridity gradient of the US (Figure 1): a deciduous broadleaf forest in Indiana (US-MMS, Roman et al., 2015) and a semi-arid shrubland in southern Arizona (US-Whs, Scott et al., 2015). For each site, we display daily evaporative fraction (*EF*), bulk surface conductance (G_s), canopy greenness, VPD, as well as total weekly precipitation. *EF* is a key measure for understanding variation in the surface energy balance (Williams & Torn, 2015), defining the proportion of available energy at the land surface partitioned as latent heat flux: $EF = LE/(LE + H)$. G_s comprises the total conductance to water fluxes from the soil and plant canopy. Overall, these time series clearly depict strong seasonal patterns at each site. At the deciduous US-MMS site, *EF* and G_s appear to closely track canopy greenness, obscuring the influence of VPD and precipitation at the annual

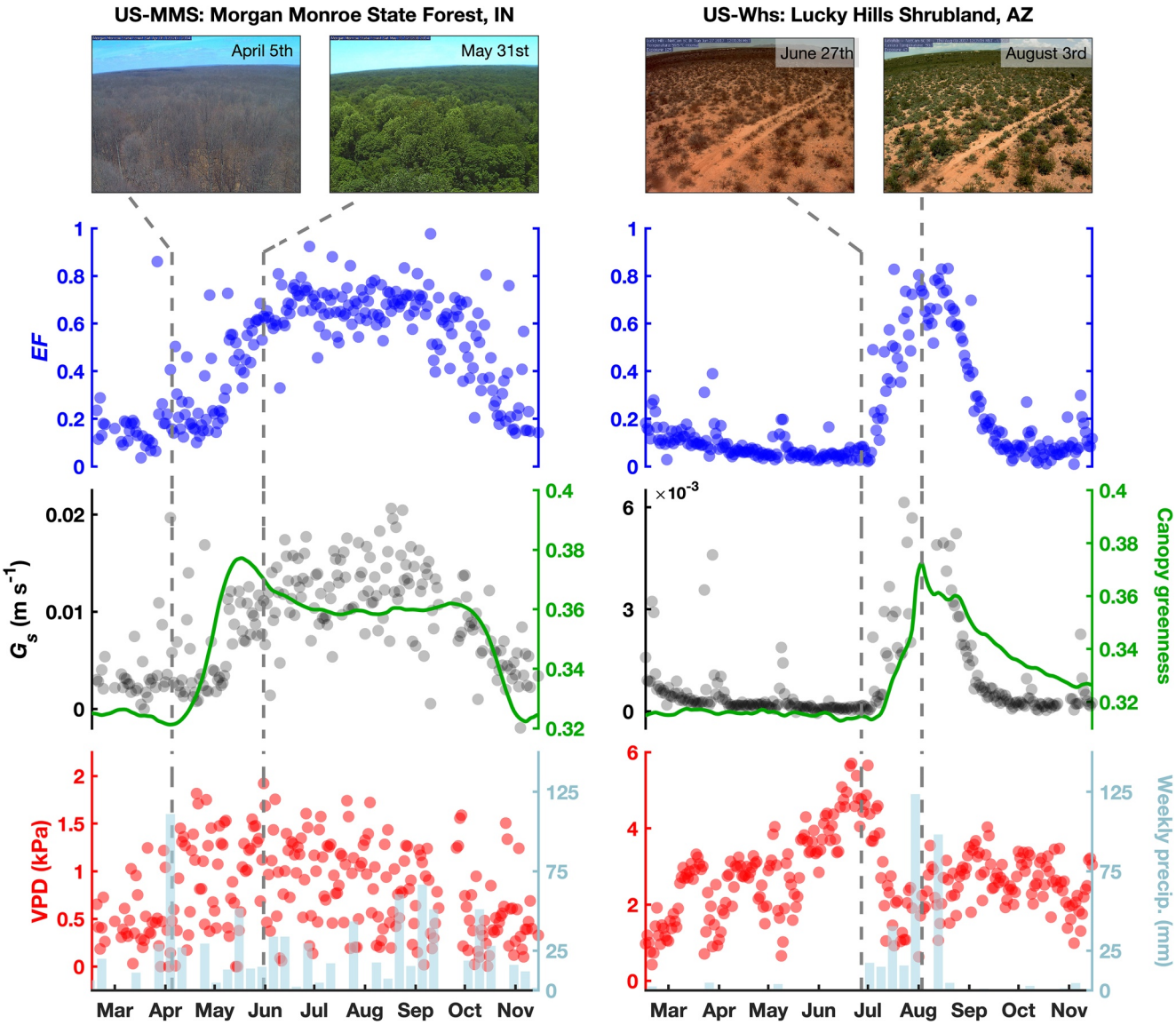

Figure 1. Example time series for two AmeriFlux sites (US-MMS and US-Whs) that span the broad climatic aridity gradient defining our study area (Table 1 and Figure 2). These time series show seasonal patterns in evaporative fraction (*EF*, blue circles), bulk surface conductance (G_s, black circles), as well as drivers with prior known influence on *ET*: canopy phenology measured by greenness from PhenoCam (green line), atmospheric vapor pressure deficit (VPD, red circles), and cumulative weekly precipitation (blue bars). Images at the top of the figure are from the *morganmonroe* and *luckyhills* PhenoCams, which display visual changes in the canopy at different times of the year. The data displayed are for 2014 at US-MMS and 2017 for US-Whs.

timescale. By comparison, at US-Whs, seasonal changes in precipitation appear to play a much larger role in driving seasonal changes in *EF* and G_s. However, none of these relationships have a clear 1:1 relationship with G_s or *EF*, and simply visualizing these time series does not account for potential mediating effects or feedbacks among different variables. Therefore, employing more complex statistical modeling to explicitly quantify the strength of these linkages is necessary for elucidating the relative controls of *ET* seasonality.

Quantifying the strength of the relationships among *EF*, G_s, greenness, and other variables (e.g., VPD, precipitation) would provide important evidence as to the primary drivers of *ET* and to seasonal changes in the surface energy balance. In this study, we focused on exploring the drivers of G_s and *EF*, using an approach comparable to structural equation modeling. Our research questions were: (a) how do the relative controls of *ET* seasonality vary among different ecosystems across a broad aridity gradient and among different PFTs, and (b) what are the most important factors to account for when predicting seasonal changes in *ET*? Our analysis includes 20 sites, 114 site

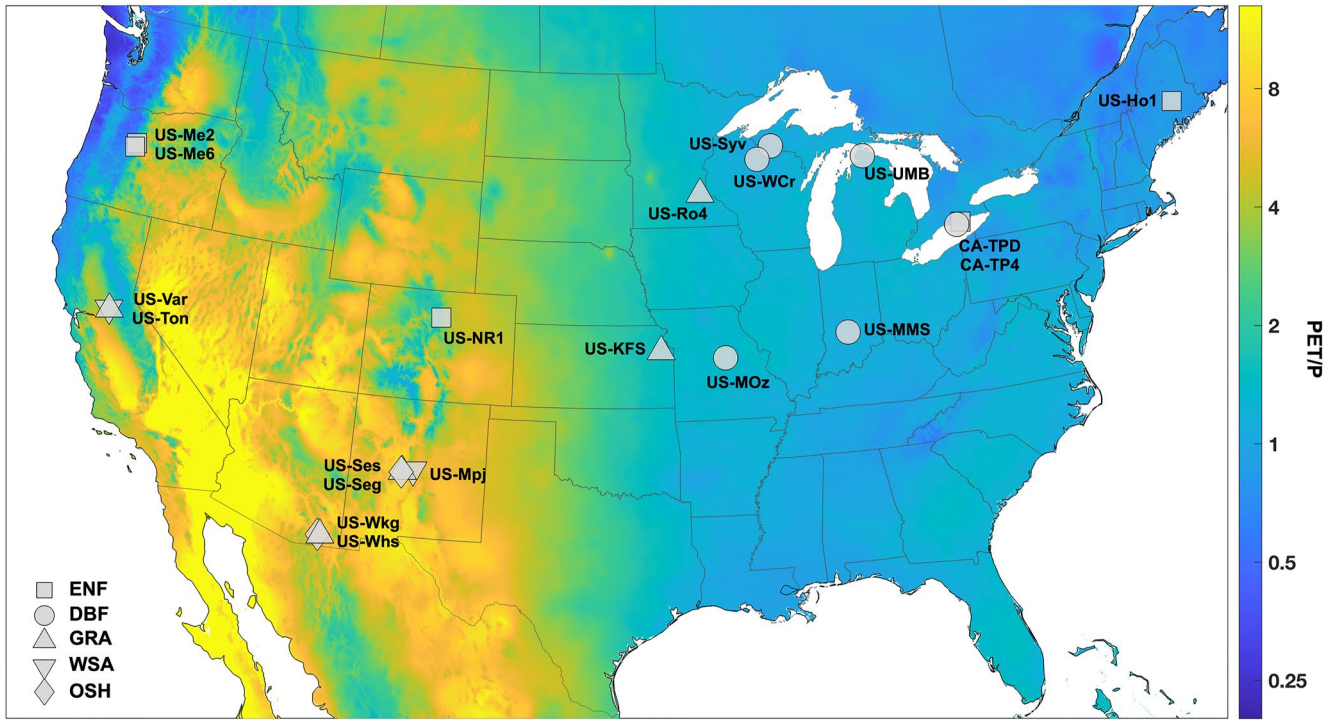

Figure 2. Geographic distribution of *PET*/*P* and our study sites in the United States and Canada. *PET*/*P* is the 30-year average (1980–2009) obtained from the Global Aridity Index data set (Trabucco & Zomer, 2019). Site-specific *PET*/*P* values are listed in Table 1. Note, *PET*/*P* is depicted on a $\log_e$ scale.

years, and spans the conterminous US, from the northeast to the southwest. Disentangling the primary drivers of seasonal patterns in *ET* among a range of energy- and water-limited ecosystems will inform our understanding of how shifts in phenological timing or hydroclimate may impact water use and deficits.

2. Methods and Materials

2.1. Study Area and Site Selection

Our study area spanned a broad climatological aridity gradient in North America (Figure 2), defined using an aridity index (*PET*/*P*). *PET*/*P* is a widely used metric that characterizes long-term atmospheric dryness, useful in aiding and understanding the drivers and impacts of changing *ET* across broad spatial areas (Greve et al., 2019), where *PET* is potential *ET* (mm) and *P* is precipitation (mm). In this study, we equate *PET* to reference evapotranspiration (ET_0), defined as expected *ET* under well-watered conditions in a short-statured grassland (Allen et al., 1998). To obtain estimates of ET_0 (and thus aridity) at the continental scale of our study area, we used the Global Aridity Index data product (Trabucco & Zomer, 2019). This data set provides 30-year average estimates of both ET_0 and P/ET_0 at a high resolution of 30 arc-seconds (~0.7 km at 40° latitude) and is derived from WorldClim v2.0 data (Fick & Hijmans, 2017). We extracted and inverted this reported P/ET_0 value as our measure of aridity at the pixel-scale for each of our study sites (Table 1). For the remainder of the paper, we refer to this inverted value as *PET*/*P*. Full details on calculating ET_0 can be found in Trabucco and Zomer (2019). As a final step, we classified energy-limited ecosystems if $PET/P < 1.5$ and water-limited ecosystems if $PET/P > 1.5$. This delineation between energy- and water-limited ecosystems is based on definitions from the United Nations FAO and World Atlas of Desertification (Spinoni et al., 2015).

We identified 20 AmeriFlux sites providing the necessary measurements needed for our analysis (Table 1, see Section 2.2 for details). Among these sites, there were five major PFTs represented: deciduous broadleaf forests, evergreen needleleaf forests, grasslands, woody savanna, and open shrubland. *PET*/*P* ranged from 0.88 at our wettest site (US-Ho1) to ~8.7 at the most arid sites (US-Seg and US-Ses). Continental patterns of *PET*/*P* were also strongly negatively correlated with mean growing season LAI ($r^2 = 0.85$, $p < 0.05$; Figure S1 in Supporting Information S1), ranging from 0.3 at US-Seg to 8.0 at CA-TP4 where $PET/P = 1.01$. We only used AmeriFlux

Table 1
Site Information for Co-Located AmeriFlux and PhenoCam Study Sites

Site	PhenoCam	PFT	Lat.	Long.	MAP (mm)	MAT (°C)	LAI (m^2/m^2)	*PET*/*P*	References	AmeriFlux data set DOI
US-Ho1	howland1	ENF	45.204	−68.740	1,070	5.3	5.7	0.88	Richardson and Hollinger (2005)	https://doi.org/10.17190/AMF/1246061
CA-TP4	turkeypointenf39	ENF	42.710	−80.357	1,036	8.0	8.0	1.01	Peichl et al. (2010)	https://doi.org/10.17190/AMF/1246012
CA-TPD	turkeypointdbf	DBF	42.635	−80.558	1,036	8.0	5.8	1.01	Beamesderfer et al. (2020)	https://doi.org/10.17190/AMF/1246152
US-Syv	sylvania	DBF	46.242	−89.348	826	3.8	4.0	1.03	Desai et al. (2005)	https://doi.org/10.17190/AMF/1246106
US-MMS	morganmonroe	DBF	39.323	−86.413	1,032	10.9	4.6	1.07	Roman et al. (2015)	https://doi.org/10.17190/AMF/1246080
US-WCr	willowcreek	DBF	45.806	−90.080	787	4.0	5.4	1.07	Cook et al. (2004)	https://doi.org/10.17190/AMF/1246111
US-UMB	umichbiological	DBF	45.560	−84.714	803	5.8	5.8	1.21	Gough et al. (2013)	https://doi.org/10.17190/AMF/1246107
US-MOz	missouriozarks	DBF	38.744	−92.200	986	12.1	3.9	1.36	Gu et al. (2016)	https://doi.org/10.17190/AMF/1246081
US-Me2	oregonMP	ENF	44.452	−121.557	523	6.3	3.0	1.41	Thomas et al. (2009)	https://doi.org/10.17190/AMF/1246076
US-Ro4	rosemountnprs	GRA	44.678	−93.072	879	6.4	3.0	1.41	Markland (2019)	https://doi.org/10.17190/AMF/1419507
US-KFS	kansas	GRA	39.056	−95.191	1,014	12.0	2.0	1.47	Brunsell et al. (2013)	https://doi.org/10.17190/AMF/1246132
US-NR1	niwot3	ENF	40.033	−105.546	800	1.5	3.7	2.29	Burns et al. (2015)	https://doi.org/10.17190/AMF/1246088
US-Me6	oregonYP	ENF	44.323	−121.608	494	7.6	1.3	2.36	Ruehr et al. (2014)	https://doi.org/10.17190/AMF/1246128
US-Ton	tonzi	WSA	38.432	−120.966	559	15.8	0.7	2.94	Ma et al. (2016)	https://doi.org/10.17190/AMF/1245971
US-Var	vaira	GRA	38.413	−120.951	559	15.8	3.5	3.02	Ma et al. (2007)	https://doi.org/10.17190/AMF/1245984
US-Mpj	usmpj	WSA	34.439	−106.238	385	10.5	1.1	4.51	Anderson-Teixeira et al. (2011)	https://doi.org/10.17190/AMF/1246123
US-Wkg	kendall	GRA	31.737	−109.942	407	15.6	0.8	5.98	Scott et al. (2010)	https://doi.org/10.17190/AMF/1246112
US-Whs	luckyhills	OSH	31.744	−110.052	320	17.6	0.5	6.75	Scott et al. (2015)	https://doi.org/10.17190/AMF/1246113
US-Ses	sevilletashrub	OSH	34.335	−106.744	275	13.7	0.3	8.68	Petrie et al. (2015)	https://doi.org/10.17190/AMF/1246125
US-Seg	sevilletagrass	GRA	34.362	−106.702	273	13.7	0.3	8.76	Petrie et al. (2015)	https://doi.org/10.17190/AMF/1246124

Note. Sites are ordered by increasing *PET*/*P*. MAP and MAT are the 30-year mean annual precipitation and mean annual temperature reported on the AmeriFlux site webpages. LAI is the mean growing season leaf area index obtained from MODIS. *PET*/*P* are grid level 30-year mean aridity indices from Trabucco and Zomer (2019). PFT codes: ENF = evergreen needleleaf forest, DBF = deciduous broadleaf forest, GRA = grassland, WSA = woody savanna, OSH = open shrubland.

sites affiliated with the PhenoCam network (https://phenocam.sr.unh.edu/webcam/) when there was a minimum of 2-years of overlap between AmeriFlux and PhenoCam time series. Meteorological and eddy covariance datasets were downloaded from the AmeriFlux web server (https://ameriflux.lbl.gov). See Table S1 in Supporting Information S1 for details.

2.2. Eddy-Covariance and Canopy Greenness Measurements

From each AmeriFlux tower, we used measurements of P, air temperature (T_a [°C]), sensible heat flux (H [W m^{-2}]), latent heat flux (LE [W m^{-2}]), relative humidity (RH [%]), and air pressure (kPa). We first filtered these tower data to only include mid-day values (10:00–14:00 local time) under the following conditions for individual half-hour or hour measurements: $T_a > 0$ and friction velocity (u_*) > 0.2 m s^{-1}. We focused on midday values where $T_a > 0$ as it was assumed transpiration was not a significant component of ET outside of these periods and this is when LE was highest at a diurnal scale. Data associated with low u_* values were excluded to remove observations with insufficient turbulence (Papale et al., 2006). We also removed days where the average mid-day H or LE was <0, to constrain our calculations of EF between 0 and 1. To exclude the confounding effects wet surfaces may have on measuring surface-atmosphere fluxes, we removed any days that had $P > 0$ within 48 hr prior to the current measurement.

To include daily estimates of vegetation activity, we used canopy greenness data from the PhenoCam public data release (V2.0; Seyednasrollah et al., 2019a, 2019b). PhenoCam datasets provide estimates of canopy "greenness" on a 1- or 3-day timestep for each site obtained from digital camera imagery. Specifically, cameras are mounted to overlook the canopy, and three-channel reg-green-blue (RGB) images are recorded typically every 30 min. Statistics summarizing RGB digital numbers (DN) at the pixel level are generated to quantify changes in canopy color over time for the image. In our analysis, we used the green-chromatic coordinate (G_{cc}) to measure canopy greenness,

$$G_{CC} = \frac{G_{DN}}{G_{DN} + R_{DN} + B_{DN}} \tag{1}$$

G_{cc} captures the relative greenness from these DN in the repeat imagery, and values typically range from 0.3 to 0.5 at most sites. We used daily estimates of G_{cc} in our analysis. Complete details and methodology for PhenoCam can be found in Seyednasrollah et al. (2019), Richardson et al. (2018), and Richardson (2019).

2.3. Processing of Eddy Covariance Datasets

For our analysis, we focused on exploring the relative controls of two measures closely related to ET: EF and bulk surface conductance (G_s). First, we chose to investigate the drivers of EF instead of ET itself because day-to-day variability in R_n can dominate the influence of other variables, and EF also captures important changes in the partitioning of the land-surface energy balance (Williams & Torn, 2015). Second, we chose to include G_s in our analysis because it directly represents the capacity for the land-surface to regulate the transfer of water to the atmosphere. G_s was estimated by inverting the Penman-Monteith model (Monteith, 1981),

$$G_s = \frac{\gamma \cdot G_a \cdot \lambda ET}{\Delta A + \rho C_p \mathrm{VPD} G_a - \lambda ET(\Delta + \gamma)} \tag{2}$$

Here, A is available energy ($H + LE = R_n - G$), ρ is air density (kg m^{-3}), C_p is specific heat of dry air (1,004.834 J K^{-1} kg^{-1}), λ is the latent heat of vapourization (J kg^{-1}, with $\lambda ET = LE$), Δ is the slope of the saturation vapor pressure curve (kPa K^{-1}), and γ is the psychrometric constant (kPa K^{-1}). VPD is atmospheric VPD and G_a is the aerodynamic conductance of water vapor transfer from the surface to the atmosphere (m s^{-1}). We used Equation 2 to estimate G_s at a daily timestep using midday data, deriving all other variables using flux tower data. We calculated G_s with the *"bigleaf"* R package (Knauer et al., 2018). We obtained values for G_a by inverting the aerodynamic equation for H,

$$G_a = H \frac{1}{\rho C_p (T_{aero} - T_a)} \tag{3}$$

Here, T_{aero} is the aerodynamic surface temperature at the source height of heat exchange in the temperature profile, which we approximated with the radiometric surface temperature by using upwelling and downwelling longwave radiation measurements (Knauer et al., 2018). Atmospheric VPD was estimated by using RH flux-tower measurements: VPD = $e^*(T_a) - e^*(T_a) \times$ RH. e^* is the saturation vapor pressure as a function of air temperature (Campbell & Norman, 1998) and RH = $e_a/e^*(T_a)$, where e_a is actual vapor pressure of the air. After these calculations, we filtered our data one final time to exclude days where $G_a < 0$ m s^{-1} or >0.5 m s^{-1}, $G_s < 0$ m s^{-1}, and

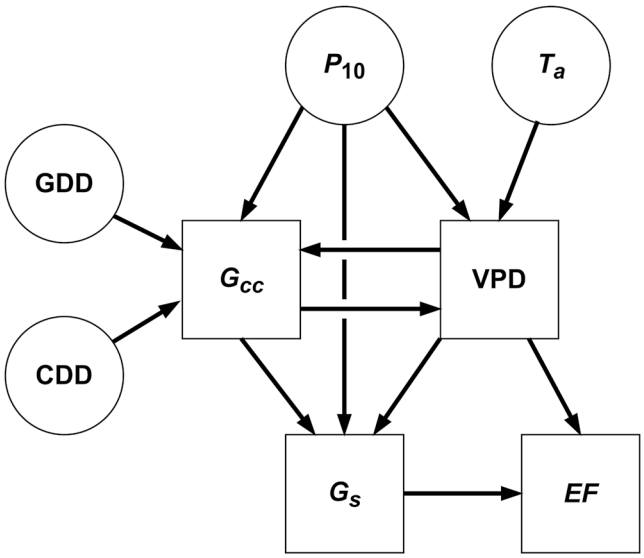

Figure 3. *a priori* conceptual path diagram for the primary drivers of bulk surface conductance (G_s) and evaporative fraction (*EF*). Circles represent exogenous variables and squares represent endogenous variables (i.e., response variables). T_a = air temperature, P_{10} = 10-day antecedent precipitation, G_{cc} is vegetation greenness as measured by PhenoCam (Equation 1), GDD and CDD are growing and chilling degree days, respectively, and VPD = atmospheric vapor pressure deficit.

VPD < 0.6 kPa. Days where VPD < 0.6 kPa were excluded to reduce the risk of these low values inflating G_s when inverting Penman-Monteith, which accounted for an average of 22% of all observations across all sites (Equation 2; Oren et al., 1999). Overall, the total number of observations remaining for statistical analysis after data filtering ranged from 290 to >3,000 among all sites.

It is reasonable to question whether it is valuable to include both G_s and *EF* simultaneously in our analysis, as we expect G_s to generally track *EF* at seasonal time scales given the intrinsic linkage between G_s and *ET*. By re-arranging and substituting Equation 3 in Equation 2, we can evaluate how G_s is theoretically related to *EF* (Equation 4),

$$G_s = \frac{\gamma \cdot G_a \cdot EF}{\Delta + \frac{\mathrm{VPD}(1-EF)}{(T_{aero}-T_a)} - EF(\Delta+\gamma)} \quad (4)$$

Equation 4 clearly demonstrates that other key factors play a role in determining the magnitude of G_s, including VPD, aerodynamic conductance (G_a), and surface-to-air temperature difference ($T_{aero} - T_a$). Thus, while G_s and *EF* may be correlated with each other, we should not expect *EF* to explain all the observed variability in G_s. Furthermore, we would not expect G_s to directly track *EF* as both measures are subject to their own uncertainties, and thus they will not perfectly match the theoretical framework of Equation 2. Therefore, we ultimately decided to include both *EF* and G_s in our analysis.

2.4. Path Analysis

Our main statistical tool for quantifying the relative importance among key drivers of G_s and *EF* was path analysis (or structural equation modeling when including latent variables, Bollen, 1989). Path analysis is a statistical modeling framework based on multiple regression theory and provides a structure for exploring the importance and strength of the causal connections among multiple response and explanatory variables. We developed an a priori path diagram capturing important causal drivers of *EF* and G_s (Figure 3).

Our path diagram (Figure 3) comprises and links together four multiple linear regression models:

$$\mathrm{VPD} = \alpha + b_1 T_a + b_2 P_{10} + b_3 G_{cc} + \varepsilon \quad (5)$$

$$G_{cc} = \alpha + b_1 \mathrm{GDD} + b_2 \mathrm{CDD} + b_3 \mathrm{VPD} + b_4 P_{10} + \varepsilon \quad (6)$$

$$G_s = \alpha + b_1 \mathrm{VPD} + b_2 P_{10} + b_3 G_{cc} + \varepsilon \quad (7)$$

$$EF = \alpha + b_1 G_s + b_2 \mathrm{VPD} + \varepsilon \quad (8)$$

Here, α and ε in Equations 5–8 are the intercept and error terms, respectively, while b represents the slope coefficients for each explanatory variable. We do not include any interactions in our regression models (e.g., VPD × P_{10}), as we account for such effects using mediation (see Section 2.5). We found consistent non-linearities among relationships involving *EF*, G_s, VPD, P_{10}, and G_{cc}. To ensure our models met required linearity assumptions, we performed $\log_e$ transformations for *EF*, G_s, VPD, and G_{cc}, as well as a square root transformation for P_{10}. Finally, all variables were standardized using a z-score prior to running our path analysis models.

Within our path diagram, we used growing degree days (GDD) and chilling degree days (CDD) as predictors for G_{cc} in place of T_a; GDD and CDD are more useful variables for modeling phenology as they capture cumulative antecedent conditions (Hänninen & Kramer, 2007). We calculated GDD and CDD using simple threshold models based on thermal forcing with parameters for start date, end date, and a base temperature for both warming and chilling. Parameters were individually selected for each PFT. We also used the cumulative 10-day sum of precipitation (i.e., P_{10}). The 10-day window was chosen because it captures both short-term rainfall pulses, important

in water-limited and arid ecosystems (Potts et al., 2006), as well as longer-term seasonal trends in precipitation that are more important for understanding in energy-limited regions (Wilson & Baldocchi, 2000). We evaluated the impact of this window length by testing 5-day, 15-day, and 30-day lengths. There was some sensitivity in our results to changing this window size, but the overall findings and inferences did not change significantly (Figure S2 in Supporting Information S1). We also chose to use precipitation instead of measures related to soil water as a measure of ecosystem water supply. While factors such as soil water potential are more physiologically relevant when characterizing plant-water availability (Liu et al., 2020; Novick et al., 2016), site-level soil water content measurements from flux tower sites are less commonly available and have varying measurement depths across sites. Therefore, precipitation likely provides a more consistent measure of site-level water availability that is comparable among all our study sites. Soil water content data was available at some sites. At these sites, we compared path analysis results between using soil water content or P_{10}, finding no meaningful differences, indicating that antecedent precipitation is adequate for capturing ecosystem water availability in our analysis (Figure S3 in Supporting Information S1). Finally, while *EF* is normalized by available energy, G_s is not. We conducted one final test to evaluate how our results may change if we controlled for available energy for G_s. To conduct this test, we filtered out all days where mean daytime net radiation (R_n) < 400 W m^{-2} and confirmed that the key findings from our study did not appreciably change when controlling for R_n (Figure S4 in Supporting Information S1).

We ensured that our path analyses met necessary statistical requirements. The path diagrams were identifiable using the *t*-rule: $t < p(p+1)/2$, where t is the number of parameters to estimate (including variances) and p is the number of variables (Bollen, 1989). Our path analysis had 10 degrees of freedom, indicating the ability of our models to uniquely identify the model parameters. Furthermore, given that our path diagram is non-recursive due to the two-way effect between G_{cc} and VPD, we confirmed that our path diagram met the required rank and order conditions (Berry, 1984). We ensured the linearity assumption between response and explanatory variables was met by using added-variable plots (Fox, 2008). All path analyses were run using the *"lavaan"* package in *R* (Rosseel, 2012). We assessed overall goodness of fit using the comparative fit index (CFI) and the standardized root mean squared residual (SRMR), as these two measures are less sensitive to variations in sample size (Chen, 2007; Hu & Bentler, 1999). CFI provides a measure of how well the path analysis model fits when compared to a baseline that assumes there is no correlation among the variables. CFI is bound between 0 and 1, with higher values indicating a stronger fit. SRMR measures the exact fit of a path analysis model, with a value 0 signaling a perfect fit and values <0.1 are generally considered to indicate a good fit. The equations for both CFI and SRMR are provided in the supplementary information (Equations S1 and S2 in Supporting Information S1). Finally, we used R^2 to evaluate goodness of fit and predictive power for each multiple linear regression in the path diagram (Equations 5–8).

2.5. The Indirect and Direct Effects on G_s

A key strength to using path analysis is the ability to quantify the total effect of a given explanatory variable on a response by considering all linkages in the diagram using "mediation" (Baron & Kenny, 1986). Specifically, mediation allows for the estimation of the indirect effects (IE) of a given explanatory variable on a response as it is mediated by another variable. This IE can then be used with a direct effect (i.e., the path coefficient directly connecting two variables) to determine the total effect of a specific explanatory variable (i.e., total effect = IE + DE). For example, using Figure 4b, the DE between G_{cc} and G_s is 0.36 (i.e., the path coefficient linking G_{cc} to G_s). IE is calculated by finding all the explanatory variables that G_{cc} links to that also connect to G_s. In this case, the only other variable is VPD, and IE is calculated as $-0.11 \times -0.43 = 0.047$ (Figure 4a). Thus, the total effect = $0.36 + 0.047 \approx 0.41$. We quantified and evaluated the total effect for P_{10}, VPD, and G_{cc} on G_s.

2.6. Quantifying Prediction Influence Among the Drivers of G_s

To aid in ranking and comparing the importance of VPD, precipitation, and canopy greenness as controls of G_s, we quantified the prediction influence (*PI*) of each variable. Specifically, we define *PI* as the improvement in prediction power gained by including the influence of a given variable in a multiple regression:

$$PI = R^2_{\text{full}} / R^2_{\text{removed}} \quad (9)$$

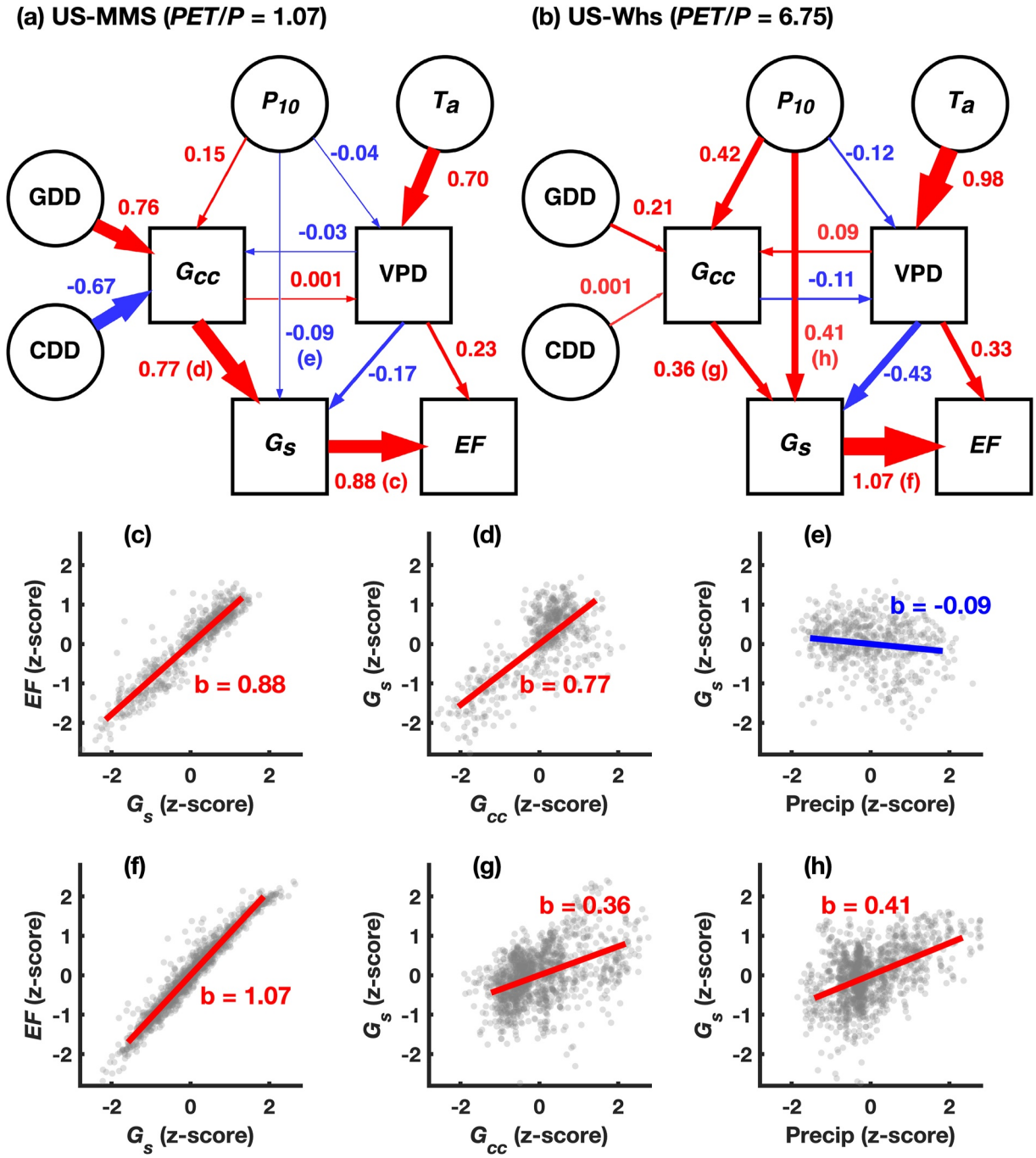

Figure 4. Examples of (a–b) path analysis results and (c–h) partial relationships for two sites broadly spanning the aridity gradient of our study area (Figures 1 and 2). In our path analysis diagrams (a–b), red arrows depict positive coefficient values while blue arrows indicate negative relationships. The beta coefficient displayed in the partial plots (c–h) is the same as the path coefficients for a given linkage displayed in (a) or (b); panels (c–e) are for US-MMS and (f–h) are for US-Whs. We chose to depict the above relationships to specifically highlight how precipitation and phenology (i.e., G_{cc}) influences G_s across the aridity gradient defining our study area.

R^2_{full} is the R^2 value for the full model with all explanatory variables included. Likewise, $R^2_{removed}$ is the R^2 when the influence of a given variable is not included. To estimate $R^2_{removed}$, rather than simply remove a specific variable completely from the multiple regression, we kept that variable in the model but randomized the order of the observations, eliminating any relationship between the chosen variable with the response, G_s. We chose this randomization approach to maintain the same number of degrees of freedom in the linear model, making R^2_{full} and $R^2_{removed}$ directly comparable. One important note regarding this approach, in some cases precipitation time series

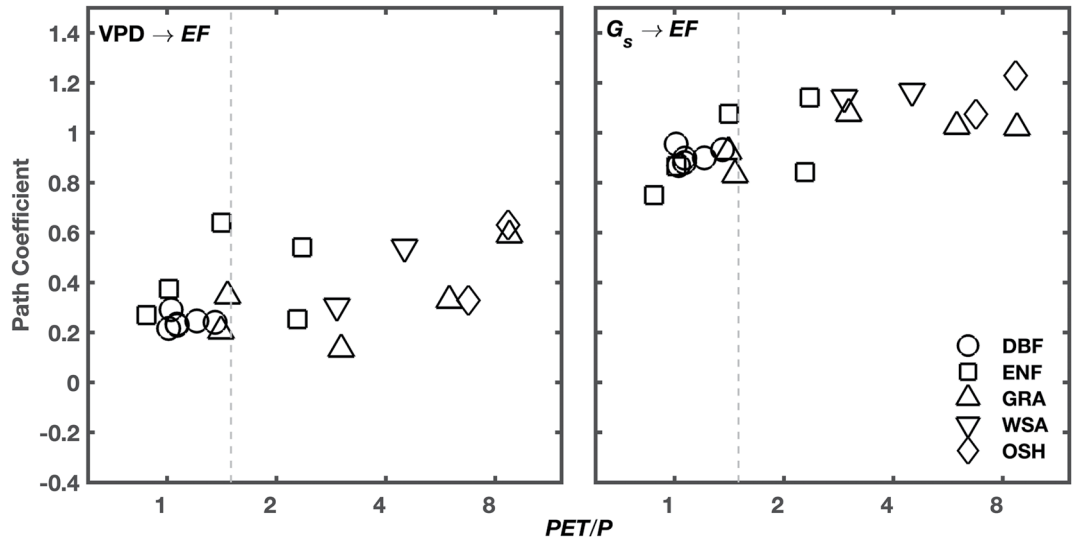

Figure 5. The path coefficients of the linkages between G_s and evapotranspiration (*EF*) and vapor pressure deficit and *EF* for each site. We plotted these coefficient values in response to *PET*/*P* (*x*-axis) and *y*-axis units are path coefficient values (e.g., Figure 4). We found no significant relationship between path values and *PET*/*P* for either variable at the $\alpha = 0.05$ significance level.

may exhibit properties of random distributions (e.g., Laio et al., 2001). The randomized precipitation time series may therefore closely resemble the observed one, resulting in potentially high uncertainty in *PI* for precipitation at some sites. However, given that seasonal precipitation is more likely to exhibit such randomness at sites where precipitation will have a lower overall effect on G_s (i.e., in energy-limited ecosystems), we do not believe that such a factor will strongly influence our results.

3. Results

Path analysis produced well-fit models at each site. Specifically, we found that CFI was >0.80 for all sites, ranging from 0.82 at an evergreen needleleaf forest site in southern Ontario (CA-TP4, *PET*/*P* = 1.01) to 0.97 at a shrubland site in southern Arizona (US-Whs, *PET*/*P* = 6.75) (Table S2 in Supporting Information S1). US-Ro4, an energy-limited grassland site (*PET*/*P* = 1.41), had the highest SRMR values (0.13). The lowest SRMR value (i.e., best fit) was 0.02, occurring at multiple sites which included a range of PFTs (Table S2 in Supporting Information S1). Finally, the R^2 for each regression model (Equations 5–8) in our path diagram indicated strong goodness-of-fit as well. While there was some variation, these R^2 values were generally high and more than 73% of the multiple regression models had an $R^2 > 0.50$ (Table S2 in Supporting Information S1).

Examining the path coefficients across all sites revealed distinct patterns regarding how the drivers of *ET* vary in relative importance across the aridity gradient. First, G_s emerged as the more important explanatory variable of *EF* relative to VPD, irrespective of PFT or *PET*/*P* (Figures 4 and 5). This importance of G_s can be demonstrated by comparing results from two sites that span the range of *PET*/*P* in our study area (Figure 1): US-MMS (*PET*/*P* = 1.07) and US-Whs (*PET*/*P* = 6.75). Specifically, for the direct effect, the path coefficient (±Std. Error) linking G_s to *EF* was 0.88 (±0.013) at US-MMS and 1.07 (±0.006) at US-Whs (Figure 4). By comparison, the path coefficients between VPD and *EF* were 0.23 (±0.013) and 0.33 (±0.006) between these same sites, respectively (Figure 4).

Although G_s was consistently ranked as the most important driver of *EF* among all our study sites (Figure 5), there was no single variable that emerged as the most important for explaining G_s. Rather, by using mediation and quantifying the total effect (i.e., DE + IE) of precipitation, VPD, and canopy greenness on G_s (see Section 2.5), we found the importance of each variable was largely dependent on site-level aridity (*PET*/*P*, Figure 6). In particular, the total effect of canopy greenness decreased with increasing *PET*/*P* (Figure 6c, $r^2 = 0.49$ and $p < 0.05$), indicating that canopy greenness had a considerably stronger effect on G_s in energy-limited ecosystems relative to water-limited ecosystems. This pattern can be illustrated by again comparing US-MMS and US-Whs (Figure 4);

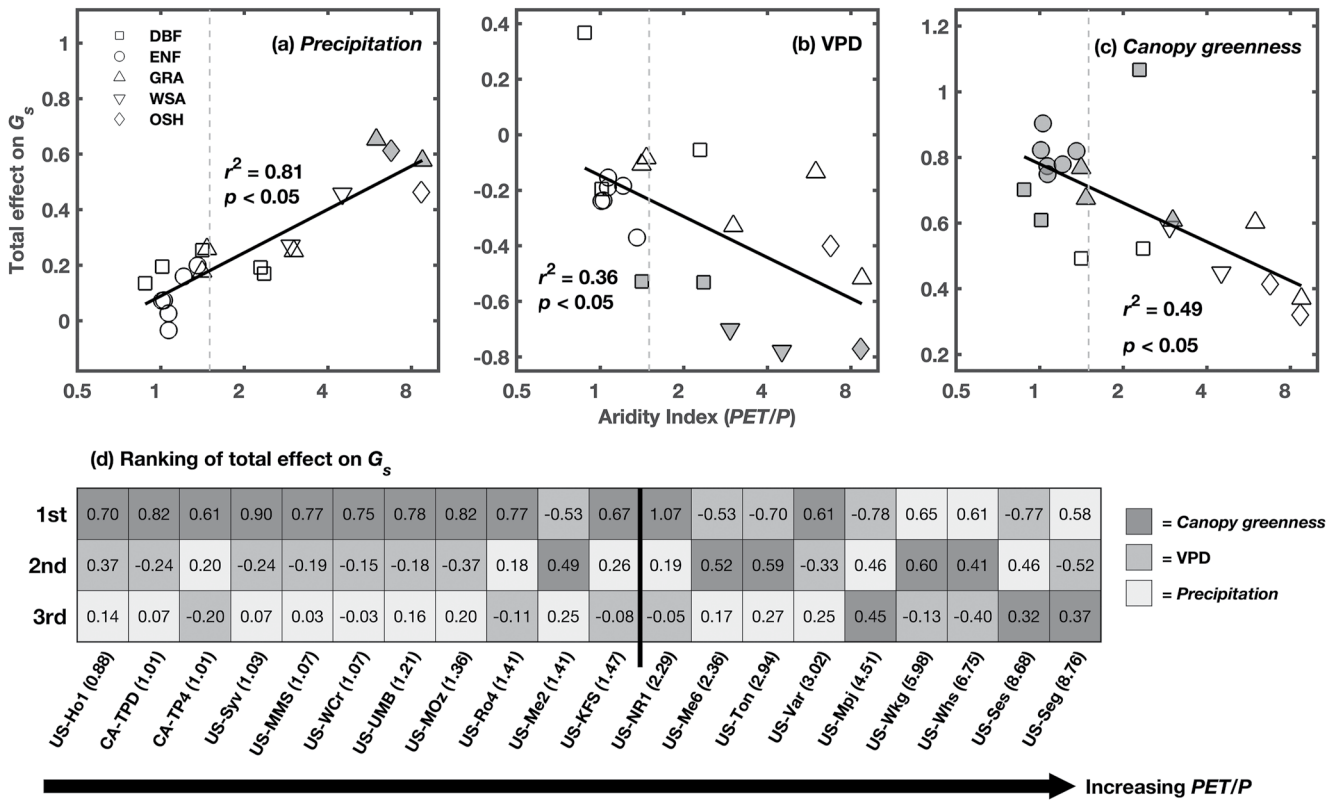

Figure 6. The total effect of (a) precipitation, (b) vapor pressure deficit (VPD), or (c) canopy greenness on G_s at all 20 study sites. The total effect of either precipitation, VPD, or canopy greenness is plotted against *PET*/*P*. If one of these three variables had the highest total effect on G_s the marker is filled in gray. In (a–c) the vertical dashed line represents the delineation between energy- and water-limited ecosystems (*PET*/*P* = 1.5). (d) Visualization of the ranking of total effects on G_s for each site, ordered by increasing *PET*/*P* (in parentheses next to each site name). Different shadings indicate different variables, and the values displayed in each cell are the total effect on G_s from the path analysis. For example, at our least-arid site, US-Ho1 (*PET*/*P* = 0.88), canopy greenness is ranked as having the highest effect (total effect = 0.70), while VPD (total effect = 0.37) and precipitation (total effect = 0.14) are ranked as having the second and third highest effects on G_s, respectively. In panel (d), the vertical black line between US-KFS and US-NR1 represents the separation between energy and water-limited ecosystems.

the path coefficients linking canopy greenness to G_s were 0.77 (±0.03) and 0.36 (±0.019) for these two sites, respectively (Figures 4d and 4g). In total, seasonal changes in canopy greenness emerged as having the highest total effect on G_s at all but one site where *PET*/*P* < 1.5 (Figure 6d). By comparison, in water-limited ecosystems, we generally found that either precipitation or VPD had the highest total effect on G_s. Specifically, precipitation had a much higher effect in the more arid ecosystems (Figure 6a; $r^2 = 0.81$ and $p < 0.05$). The total effect of VPD was relatively high at many sites, with a significant pattern indicating that the magnitude of the effect of VPD was higher in water-limited systems (Figure 6b; $r^2 = 0.36$, $p < 0.05$); VPD either had the highest or second highest total effect at 14 out of 20 sites (Figure 6d).

While our path analysis provided key information for understanding how the drivers of G_s may vary among ecosystems, the results from it do not indicate the importance of accounting for each variable when predicting seasonal patterns in G_s. To address this limitation, we quantified the prediction influence for precipitation, VPD, and canopy greenness for each site using Equation 9. We found that accounting for canopy greenness was necessary to successfully predict seasonal patterns in G_s (Figure 7), and thus *ET*. In energy-limited ecosystems, the average prediction influence was 920%, indicating that including the influence of greenness as an explanatory variable improved model predictions by a significant amount. In water-limited ecosystems this influence was considerably less, averaging 145%. The prediction influence of VPD or precipitation was generally low (<200%) relative to greenness.

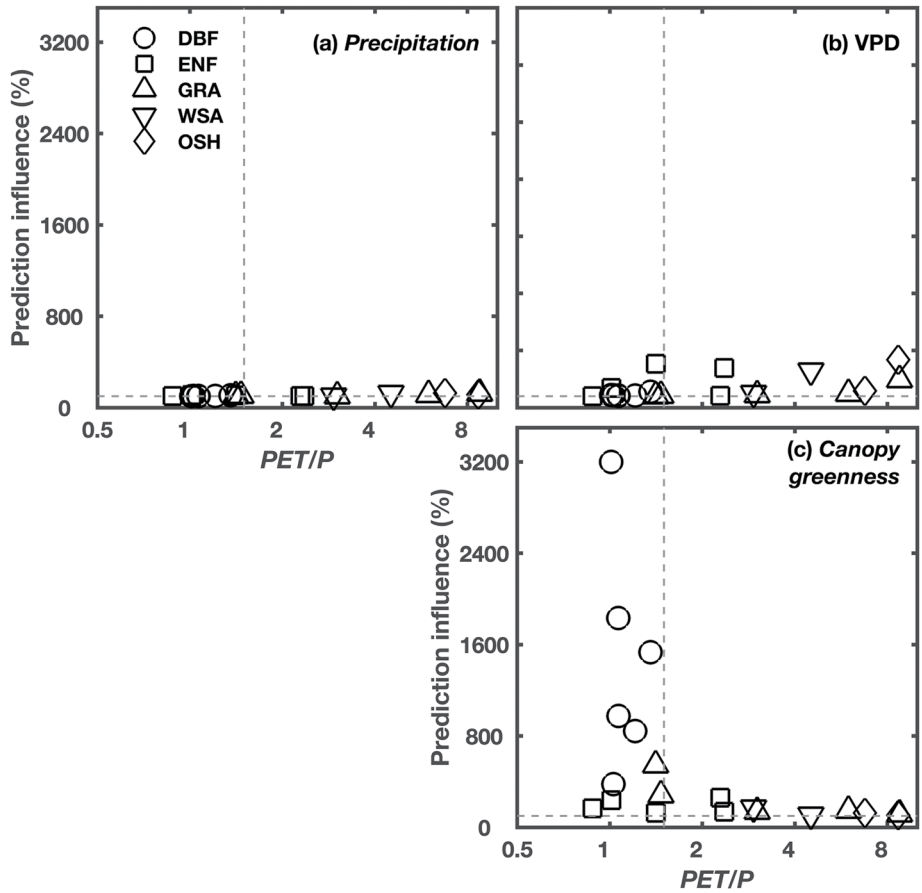

Figure 7. Prediction influence of precipitation, vapor pressure deficit, and canopy greenness (Equation 9). Prediction influence measures the change in R^2 when each of these variables is included in a multiple regression model predicting G_s. For example, a value of 800% for canopy greenness indicates that there is an eightfold increase in R^2 when greenness is included as an explanatory variable. The horizontal dashed line in all three panels represents 100% (i.e., no difference).

4. Discussion

To understand how the drivers of *ET* vary in relative strength among different ecosystems and climatic regimes, we leveraged daily time series data from 20 AmeriFlux and PhenoCam sites that span a broad climatological aridity gradient (*PET*/*P*) in the US We used path analysis to model a relatively simple ecological network characterizing the linkages among multiple response and explanatory variables. We found clear evidence that bulk surface conductance (G_s) had the highest relative control over *EF*, with VPD having an important, yet secondary effect. However, whereas the strong influence of G_s over *EF* was consistent among all sites, the underlying drivers of G_s notably varied in importance, particularly in response to site-level *PET*/*P*. Specifically, at sites where *ET* is limited primarily by energy availability (i.e., energy-limited ecosystems), we found that canopy greenness had the strongest effect on G_s relative to meteorological factors, such as VPD or precipitation. In the remainder of this discussion, we highlight and disentangle how the controls of G_s—and thus *EF*—vary in strength and importance among different ecosystems, with a particular focus on the role of phenology.

4.1. How do the Relative Controls of G_s Vary Among Ecosystems?

Seasonal changes in canopy greenness measured by PhenoCam G_{cc} had the highest total effect on G_s at most of our study sites (60%), implying that phenology acts as a key driver of G_s and *EF* in some, but not all, ecosystems. Furthermore, we found that this strong influence of greenness did not occur randomly among sites; instead, it was much more prominent in energy-limited ecosystems (i.e., $PET/P < 1.5$). In energy-limited ecosystems there is generally abundant and stable soil moisture in the root zone, particularly during the early part of the growing season

(Wilson et al., 2000). However, this root-zone soil moisture is effectively unavailable for evaporation, particularly when the soil surface begins to dry (Daikoku et al., 2008; Idso et al., 1974). Plants provide the hydraulic architecture to transport this soil moisture to the atmosphere via water loss as stomata open during photosynthesis (Sakai et al., 1997; Tyree & Ewers, 1991; Wilson & Baldocchi, 2000). As a result, canopy greenness—acting as a proxy measure for transpiration occurring under photosynthesis—emerges as having the strongest effect on G_s in energy-limited ecosystems. This finding is not necessarily surprising, given that many of the energy-limited sites used in this study are from deciduous broadleaf forests (Fitzjarrald et al., 2001; Schwartz, 1992). Likewise, the relationship between greenness and G_s may be confounded by physiological feedbacks among VPD and stomatal aperture; stomata close to prevent water loss during periods of high VPD, thereby ultimately decreasing G_s even though canopy greenness may not decrease in unison (Grossiord et al., 2020; Novick et al., 2016; Oren et al., 1999). Additionally, increasing VPD and decreasing soil moisture can influence the timing of leaf senescence and green-down in some ecosystems, and thus VPD may have a higher effect on G_s at certain parts of the year (Seyednasrollah et al., 2020; Zavaleta et al., 2003). Nevertheless, at seasonal time scales, we consider VPD to have secondary influence as a control of G_s compared to vegetation phenology in energy-limited ecosystems, as the importance of VPD is dependent on vegetation status.

A second key pattern highlighted by our results is that this effect of greenness on G_s occurred among multiple different PFTs, including deciduous broadleaf, evergreen needleleaf forests, and grasslands. While linkages between phenology and shifts in G_s or *ET* have been well established for decades in deciduous broadleaf forests (Blanken & Black, 2004; Sakai et al., 1997), we provide clear evidence extending this linkage to other ecosystems and PFTs. For example, we found strong linkages between canopy greenness and G_s in evergreen needleleaf forests, providing evidence for a direct and clear linkage between photosynthetic activity and water use in these systems (Bowling et al., 2018; Seyednasrollah et al., 2021; Stoy et al., 2006). Furthermore, we found that this strong effect of greenness was not limited to only energy-limited systems. In a water-limited Mediterranean grassland site in central California (US-Var, $PET/P = 1.98$), greenness was ranked as more important than VPD or precipitation (Figure 6). At this site, the growing season occurs during the spring rather than summer months; peak *ET* and greenness occurs at approximately May 10th in a given year, when soil water is non-limiting and air temperature is relatively mild (Baldocchi et al., 2021). Thus, even though $PET/P > 1.5$ at annual time scales, greenness still has a large influence on G_s during periods of the year when soil water is non-limiting. Comparatively, during the hot and dry summer months both the vegetation senesces and G_s decreases due the lack of moisture availability (Baldocchi et al., 2010). This result from a water-limited ecosystem highlights that the strong influence of greenness is not limited to only certain PFTs. Instead, seasonal shifts in photosynthetic activity acts as a key regulator and control of G_s through changes in stomatal aperture, and this linkage can be measured and modeled using measurements of canopy greenness.

Canopy greenness had a much smaller effect on G_s in water-limited regions, with either antecedent 10-day precipitation or VPD having the strongest total effect on G_s (Figure 6). This relatively small effect of greenness on G_s in water-limited ecosystems is primarily a product of variations in LAI that accompany *PET*/*P* (Table 1 and Figure S1 in Supporting Information S1). Specifically, in water-limited ecosystems, bare soil comprises a much higher proportion of land cover for most of the year, leading to surface evaporation being a more substantial contribution to *ET* relative to transpiration (Scott et al., 2021; Villegas et al., 2010; Wang et al., 2014). Consequently, significant water fluxes can occur regardless of vegetation status, resulting in G_s being decoupled from seasonal phenological signals of vegetation greening. Examples of this decoupling occur during the North American monsoon. Specifically, green-up and subsequent transpiration in semi-arid systems is triggered by monsoonal precipitation (Matsui et al., 2005). However, there are significant increases in surface evaporation as wetting of the soil surface (i.e., 0–50 mm) occurs well before green-up, and transpiration may not happen for several days-to-weeks until water infiltrates into the root zone (Kurc & Small, 2004; Scott et al., 2006). Vegetation seasonality is therefore not acting as a first-order control of G_s in water-limited ecosystems. Additionally, it should be noted that species composition or PFTs may be playing a role in driving how decoupled phenology appears to be from *ET* in water-limited ecosystems. Specifically, at two shrubland sites (US-Whs and US-Ses), the influence of phenology is notably lower relative to a grassland site (US-Wkg), and this difference may be due to shrubs having a more delayed decline in senescence than in grasslands (Yan et al., 2019).

In general, the lack of influence of greenness in water-limited ecosystems compared to energy-limited ecosystems was fairly surprising for several reasons. First, there are clear examples of G_s or *ET* or plant productivity

closely tracking phenological signals of greenness in these systems (e.g., Figure 1, Vivoni et al., 2008; Yan et al., 2019). Second, the ratio of transpiration to *ET* (i.e., *T*/*ET*) can sometimes peak as high as 60% to >80% in water-limited ecosystems, indicating plant physiological activity plays a key role in governing *ET* for at least parts of the year (Raz-Yaseef et al., 2012; Scott & Biederman, 2017). Finally, plants in semi-arid regions can provide access to deeper soil water that is unavailable for surface evaporation, enhancing transpiration and G_s (Cavanaugh et al., 2011; Scott et al., 2006). Discrepancies between our results and past studies may be due to differences in scale; by evaluating the time series at daily timestep, any divergences between the timing of green-up and seasonal shifts in G_s will be more evident. For example, at an open shrubland site in southeastern Arizona (US-Whs, $PET/P = 6.75$), shifts in increasing *EF* and precipitation clearly occur well before green-up (Figure 1), resulting in greenness having little effect on G_s (Figure 4). Likewise, senescence in shrublands lags behind more immediate response of G_s to decreased precipitation (Figure 1). Finally, this lack of phenological influence may also be due in part to a decoupling of vegetation and *ET* or plant productivity due to water limitations during long inter-storm periods in the growing season; in general, greenness is slower to respond to precipitation pulses in such ecosystems (Yan et al., 2019). Thus, while vegetation can play an important role in regulating G_s during the growing season in water-limited regions (Scott et al., 2021), it is a less informative predictor of G_s relative to precipitation.

4.2. The Varying Importance of Vegetation Phenology as a Driver of G_s: Implications for Understanding Present and Future Changes in Ecosystem Water Fluxes

Our analysis highlights that vegetation phenology acted as the primary control of G_s, but only in energy-limited ecosystems. As indicated in the previous section of this discussion, this lack of importance of phenology in water-limited ecosystems was surprising, and there are several implications associated with this finding. First, seasonal patterns in *ET* and the partitioning of the surface energy balance are driven primarily by climatic factors, rather than biological or physiological controls in these regions. In particular, this indicates that *ET* may become increasingly sensitive to atmospheric VPD as climatological aridity increases (Baldocchi et al., 2022). Such decoupling from the land surface ultimately implies that the capacity for vegetation phenology to mediate this sensitivity of *ET* to climate will become increasingly diminished (e.g., Zavaleta et al., 2003). Furthermore, drylands are expected to expand regionally under many future climate change scenarios (Huang et al., 2016; Yao et al., 2020). Expansion of such water-limited ecosystems suggests that the phenology may play a less important role in governing the surface energy balance over broader spatial regions as time goes on, potentially affecting planetary-boundary layer dynamics and mesoscale weather patterns (Hiestand & Carleton, 2020). Finally, while the influence of phenology is less at water-limited sites relative to sites in energy-limited ecosystems, it is not negligible. However, there may be an LAI threshold of fractional vegetation cover where the influence of phenology is effectively nil. Identifying such a threshold will likely be important as many regions continue to experience increasing aridity.

The significant influence phenology has on G_s in energy-limited ecosystems also comes with some important implications. In particular, the strong linkage from greenness $\rightarrow G_s \rightarrow EF$ directly implies that phenology plays a significant role regulating seasonal variability in the surface energy balance, with potential implications for land-atmosphere interactions in energy-limited ecosystems. Specifically, by modeling *EF* in our path analysis, we provide direct evidence that the partitioning of available energy closely tracks canopy greenness through G_s in these ecosystems. Our results share important parallels with past studies. For example, similar linkages between canopy greenness and seasonal variations in the land-surface energy balance have been identified in deciduous broadleaf forests, where distinct seasonal shifts of the Bowen ratio (*H*/*LE*) occur in response to leaf emergence occur (Fitzjarrald et al., 2001; Moon et al., 2020; Schwartz, 1992). Furthermore, recent work has established strong seasonal correlations between seasonal *EF* and LAI, indicating vegetation plays a critical role in governing land-atmosphere coupling across a broad range of US ecosystems (Williams & Torn, 2015). Our findings expand on these past studies by explicitly quantifying and identifying key regional differences in the importance of phenology, and to our knowledge, there are few studies that have identified similar regional patterns (e.g., Guillevic et al., 2002). Broadscale, regional differences in the effect of phenology on *ET* can have considerable impacts on land-atmosphere coupling and synoptic-scale atmospheric dynamics. For example, there is evidence that strong phenological patterns in aspen-dominated boreal forest ecosystems in central Canada enhance *ET* and *EF* relative to bordering evergreen needleleaf forests, ultimately influencing regional precipitation patterns and surface warming (Hogg et al., 2000). As an additional illustration for regional-scale implications, in the U.S.

Midwest differing phenological effects on *ET* between deciduous broadleaf forests and neighboring croplands influenced the likelihood of convective precipitation (Carleton et al., 2008; Hiestand & Carleton, 2020).

We have discussed how continental-scale variability in the drivers of *ET* are important for understanding shifts in the land-surface energy balance among different hydroclimatic regimes. However, this finding by itself does not directly address the importance of accounting for such patterns when predicting seasonal variations in *ET*. As a final piece to this analysis, we found that including vegetation phenology is essential for successfully predicting the complete seasonal trajectory of G_s in energy-limited ecosystems. Specifically, we found that including canopy greenness in our multiple linear regression models to predict G_s (Equation 7) ultimately improved $R^2 > 300\%$; the prediction influence of both VPD and precipitation was comparatively less at most sites (Figure 7). While this finding is not necessarily novel (e.g., Granier et al., 2000; Wilson & Baldocchi, 2000), it does further cement the inference that accounting for regional variations in phenology-*ET* relationships can have significant influence on accurately forecasting land-surface and meteorological processes (Fischer et al., 2007; Guillevic et al., 2002; Lu & Shuttleworth, 2002; Puma et al., 2013). The results also highlight the importance of controlling for greenness or LAI when attempting to disentangle the effects of soil moisture and/or VPD conductance or carbon uptake at the ecosystem-scale. It is expected that both the timing of green-up and growing-season length will be sensitive to future warming, particularly in energy-limited ecosystems where vegetation phenology was identified as the most important driver of G_s (Migliavacca et al., 2012; Seyednasrollah et al., 2020). In these systems, shifts to earlier green-up and longer growing seasons could lead to depletion of soil water through increased *ET*, ultimately enhancing surface warming and affecting regional climates (Lian et al., 2020; Miralles et al., 2014).

5. Conclusions

Through a data synthesis using mid-day eddy covariance measurements from AmeriFlux and PhenoCam greenness data, we elucidated how vegetation phenology varies in importance as a control of bulk surface conductance (G_s) across a broad climatic gradient. We used path analysis to compare and evaluate the causal linkages among G_s, VPD, precipitation, and canopy greenness. Using the path coefficients from this approach, we found clear patterns that the drivers of G_s (and thus *ET*) vary across a continental-scale aridity gradient. Specifically, our findings highlight that seasonal greenness had the strongest influence in energy-limited ecosystems, regardless of specific PFT, indicating that phenology plays a key role in governing seasonal patterns of the surface energy balance in many ecosystems. By comparison, phenology consistently had relatively low importance in water-limited ecosystems; instead, precipitation had a significantly higher effect on G_s. Finally, we found that accounting for vegetation phenology in predictive models is critical for successfully anticipating seasonality in *ET* in energy-limited ecosystems.

Data Availability Statement

AmeriFlux data used in this analysis are available at https://ameriflux.lbl.gov/, and the dataset citations for each site are provided in Table 1. PhenoCam datasets are from the V2.0 public data release available on the ORNL DAAC (https://doi.org/10.3334/ORNLDAAC/1674). The code used to conduct this analysis is available on GitHub via Zenodo (https://doi.org/10.5281/zenodo.6558541).

Acknowledgments
This research was supported by NSF Macrosystems Biology awards DEB-1702697 to A. D. Richardson, DEB-1702627 to M. A. Friedl, and DEB-1702727 to S. Frolking. In addition, funding for AmeriFlux data resources was provided by the U.S. Department of Energy's Office of Science. We also thank our many PhenoCam site collaborators. Additional site-specific acknowledgments can be found in Table S1 in Supporting Information S1.

References

Allen, R. G., Pereira, L. S., Raes, D., & Smith, M. (1998). Crop Evapotranspiration: Guidelines for Computing Crop Water Requirements: FAO Irrigation and Drainage Paper 56. Retrieved from http://www.fao.org/3/X0490E/X0490E00.htm

Anderson-Teixeira, K. J., Delong, J. P., Fox, A. M., Brese, D. A., & Litvak, M. E. (2011). Differential responses of production and respiration to temperature and moisture drive the carbon balance across a climatic gradient in New Mexico. *Global Change Biology*, *17*(1), 410–424. https://doi.org/10.1111/j.1365-2486.2010.02269.x

Baldocchi, D., Chen, Q., Chen, X., Ma, S., Miller, G., Ryu, Y., & Battles, J. (2010). The dynamics of energy, water and carbon fluxes in a blue oak (Quercus douglasii) savanna in California, USA. In *Ecosystem function in global savannas: Measurement and modeling at landscape to global scales* (1st ed., pp. 135–151). CRC/Taylor and Francis. https://doi.org/10.1201/b10275

Baldocchi, D., Ma, S., & Verfaillie, J. (2021). On the inter- and intra-annual variability of ecosystem evapotranspiration and water use efficiency of an oak savanna and annual grassland subjected to booms and busts in rainfall. *Global Change Biology*, *27*(2), 359–375. https://doi.org/10.1111/gcb.15414

Baldocchi, D. D., Keeney, N., Rey-Sanchez, C., & Fisher, J. B. (2022). Atmospheric humidity deficits tell us how soil moisture deficits down-regulate ecosystem evaporation. *Advances in Water Resources*, *159*, 104100. https://doi.org/10.1016/j.advwatres.2021.104100

Baron, R. M., & Kenny, D. A. (1986). The moderator–mediator variable distinction in social psychological research: Conceptual, strategic, and statistical considerations. *Journal of Personality and Social Psychology*, *51*(6), 1173–1182. https://doi.org/10.1037/0022-3514.51.6.1173

Barr, A. G., Black, T. A., Hogg, E. H., Griffis, T. J., Morgenstern, K., Kljun, N., et al. (2007). Climatic controls on the carbon and water balances of a boreal aspen forest, 1994–2003. *Global Change Biology*, *13*(3), 561–576. https://doi.org/10.1111/j.1365-2486.2006.01220.x

Beamesderfer, E. R., Arain, M. A., Khomik, M., & Brodeur, J. J. (2020). The impact of seasonal and annual climate variations on the carbon uptake capacity of a deciduous forest within the Great Lakes region of Canada. *Journal of Geophysical Research: Biogeosciences*, *125*(9), e2019JG005389. https://doi.org/10.1029/2019JG005389

Berry, W. D. (1984). *Nonrecursive causal models*. Sage Publications.

Blanken, P. D., & Black, T. A. (2004). The canopy conductance of a boreal aspen forest, Prince Albert National Park, Canada. *Hydrological Processes*, *18*(9), 1561–1578. https://doi.org/10.1002/hyp.1406

Bollen, K. (1989). *Structural equations with latent variables*. Wiley.

Bowling, D. R., Logan, B. A., Hufkens, K., Aubrecht, D. M., Richardson, A. D., Burns, S. P., et al. (2018). Limitations to winter and spring photosynthesis of a Rocky Mountain subalpine forest. *Agricultural and Forest Meteorology*, *252*, 241–255. https://doi.org/10.1016/j.agrformet.2018.01.025

Brunsell, N. A., Nippert, J. B., & Buck, T. L. (2013). Impacts of seasonality and surface heterogeneity on water-use efficiency in mesic grasslands. *Ecohydrology*. https://doi.org/10.1002/eco.1455

Burns, S. P., Blanken, P. D., Turnipseed, A. A., Hu, J., & Monson, R. K. (2015). The influence of warm-season precipitation on the diel cycle of the surface energy balance and carbon dioxide at a Colorado subalpine forest site. *Biogeosciences*, *12*(23), 7349–7377. https://doi.org/10.5194/bg-12-7349-2015

Campbell, G. S., & Norman, J. M. (1998). *An introduction to environmental biophysics* (2nd ed.). Springer. https://doi.org/10.1007/978-1-4612-1626-1

Carleton, A. M., Travis, D. J., Adegoke, J. O., Arnold, D. L., & Curran, S. (2008). Synoptic circulation and land surface influences on convection in the Midwest U.S. "Corn Belt" during the summers of 1999 and 2000. Part II: Role of vegetation boundaries. *Journal of Climate*, *21*(15), 3617–3641. https://doi.org/10.1175/2007JCLI1584.1

Cavanaugh, M. L., Kurc, S. A., & Scott, R. L. (2011). Evapotranspiration partitioning in semiarid shrubland ecosystems: A two-site evaluation of soil moisture control on transpiration. *Ecohydrology*, *4*(5), 671–681. https://doi.org/10.1002/eco.157

Chen, F. F. (2007). Sensitivity of goodness of fit indexes to lack of measurement invariance. *Structural Equation Modeling: A Multidisciplinary Journal*, *14*(3), 464–504. https://doi.org/10.1080/10705510701301834

Cook, B. D., Davis, K. J., Wang, W., Desai, A., Berger, B. W., Teclaw, R. M., et al. (2004). Carbon exchange and venting anomalies in an upland deciduous forest in northern Wisconsin, USA. *Agricultural and Forest Meteorology*, *126*(3–4), 271–295. https://doi.org/10.1016/j.agrformet.2004.06.008

Daikoku, K., Hattori, S., Deguchi, A., Aoki, Y., Miyashita, M., Matsumoto, K., et al. (2008). Influence of evaporation from the forest floor on evapotranspiration from the dry canopy. *Hydrological Processes*, *22*(20), 4083–4096. https://doi.org/10.1002/hyp.7010

Desai, A. R., Bolstad, P. V., Cook, B. D., Davis, K. J., & Carey, E. v. (2005). Comparing net ecosystem exchange of carbon dioxide between an old-growth and mature forest in the upper Midwest, USA. *Agricultural and Forest Meteorology*, *128*(1–2), 33–55. https://doi.org/10.1016/j.agrformet.2004.09.005

Fick, S. E., & Hijmans, R. J. (2017). WorldClim 2: New 1-km spatial resolution climate surfaces for global land areas. *International Journal of Climatology*, *37*(12), 4302–4315. https://doi.org/10.1002/joc.5086

Fischer, E. M., Seneviratne, S. I., Vidale, P. L., Lüthi, D., & Schär, C. (2007). Soil moisture–atmosphere interactions during the 2003 European summer heat wave. *Journal of Climate*, *20*(20), 5081–5099. https://doi.org/10.1175/JCLI4288.1

Fitzjarrald, D. R., Acevedo, O. C., & Moore, K. E. (2001). Climatic consequences of leaf presence in the eastern United States. *Journal of Climate*, *14*(4), 598–614. https://doi.org/10.1175/1520-0442(2001)014<0598:CCOLPI>2.0.CO;2

Fox, J. (2008). *Applied regression analysis and generalized linear models* (2nd ed.). Sage Publications.

Glenn, E. P., Nagler, P. L., & Huete, A. R. (2010). Vegetation index methods for estimating evapotranspiration by remote sensing. *Surveys in Geophysics*, *31*(6), 531–555. https://doi.org/10.1007/s10712-010-9102-2

Gough, C. M., Hardiman, B. S., Nave, L. E., Bohrer, G., Maurer, K. D., Vogel, C. S., et al. (2013). Sustained carbon uptake and storage following moderate disturbance in a Great Lakes forest. *Ecological Applications*, *23*(5), 1202–1215. https://doi.org/10.1890/12-1554.1

Granier, A., Loustau, D., & Bréda, N. (2000). A generic model of forest canopy conductance dependent on climate, soil water availability and leaf area index. *Annals of Forest Science*, *57*(8), 755–765. https://doi.org/10.1051/forest:2000158

Greve, P., Roderick, M. L., Ukkola, A. M., & Wada, Y. (2019). The aridity Index under global warming. *Environmental Research Letters*, *14*(12), 124006. https://doi.org/10.1088/1748-9326/ab5046

Grossiord, C., Buckley, T. N., Cernusak, L. A., Novick, K. A., Poulter, B., Siegwolf, R. T. W., et al. (2020). Plant responses to rising vapor pressure deficit. *New Phytologist*, *226*(6), 1550–1566. https://doi.org/10.1111/nph.16485

Gu, L., Pallardy, S. G., Yang, B., Hosman, K. P., Mao, J., Ricciuto, D., et al. (2016). Testing a land model in ecosystem functional space via a comparison of observed and modeled ecosystem flux responses to precipitation regimes and associated stresses in a Central U.S. forest. *Journal of Geophysical Research: Biogeosciences*, *121*(7), 1884–1902. https://doi.org/10.1002/2015JG003302

Guillevic, P., Koster, R. D., Suarez, M. J., Bounoua, L., Collatz, G. J., Los, S. O., & Mahanama, S. P. P. (2002). Influence of the interannual variability of vegetation on the surface energy balance—A global sensitivity study. *Journal of Hydrometeorology*, *3*(6), 617–629. https://doi.org/10.1175/1525-7541(2002)003<0617:IOTIVO>2.0.CO;2

Han, Q., Liu, Q., Wang, T., Wang, L., Di, C., Chen, X., et al. (2020). Diagnosis of environmental controls on daily actual evapotranspiration across a global flux tower network: The roles of water and energy. *Environmental Research Letters*, *15*(12), 124070. https://doi.org/10.1088/1748-9326/abcc8c

Hänninen, H., & Kramer, K. (2007). A framework for modelling the annual cycle of trees in boreal and temperate regions. *Silva Fennica*, *4*(1), 167–205. https://doi.org/10.14214/sf.313

Hiestand, M. P., & Carleton, A. M. (2020). Growing-season synoptic and phenological controls on heat fluxes over forest and cropland sites in the Midwest U.S. Corn Belt. *Journal of Applied Meteorology and Climatology*, *59*(3), 381–400. https://doi.org/10.1175/JAMC-D-19-0019.1

Hogg, E. H., Price, D. T., & Black, T. A. (2000). Postulated feedbacks of deciduous forest phenology on seasonal climate patterns in the western Canadian interior. *Journal of Climate*, *13*(24), 4229–4243. https://doi.org/10.1175/1520-0442(2000)013<4229:PFODFP>2.0.CO;2

Hu, L., & Bentler, P. M. (1999). Cutoff criteria for fit indexes in covariance structure analysis: Conventional criteria versus new alternatives. *Structural Equation Modeling: A Multidisciplinary Journal*, *6*(1), 1–55. https://doi.org/10.1080/10705519909540118

Huang, J., Yu, H., Guan, X., Wang, G., & Guo, R. (2016). Accelerated dryland expansion under climate change. *Nature Climate Change*, *6*(2), 166–171. https://doi.org/10.1038/nclimate2837

Idso, S. B., Reginato, R. J., Jackson, R. D., Kimball, B. A., & Nakayama, F. S. (1974). The three stages of drying of a field soil. *Soil Science Society of America Journal*, *38*(5), 831–837. https://doi.org/10.2136/sssaj1974.03615995003800050037x

Kim, Y., & Wang, G. (2007). Impact of vegetation feedback on the response of precipitation to antecedent soil moisture anomalies over North America. *Journal of Hydrometeorology*, *8*(3), 534–550. https://doi.org/10.1175/JHM612.1

Knauer, J., El-Madany, T. S., Zaehle, S., & Migliavacca, M. (2018). Bigleaf—An R package for the calculation of physical and physiological ecosystem properties from eddy covariance data. *PLoS One*, *13*(8), e0201114. https://doi.org/10.1371/journal.pone.0201114

Konings, A. G., Katul, G. G., & Porporato, A. (2010). The rainfall-no rainfall transition in a coupled land-convective atmosphere system. *Geophysical Research Letters*, *37*(14), L14401. https://doi.org/10.1029/2010GL043967

Kurc, S. A., & Small, E. E. (2004). Dynamics of evapotranspiration in semiarid grassland and shrubland ecosystems during the summer monsoon season, central New Mexico. *Water Resources Research*, *40*(9), W09305. https://doi.org/10.1029/2004WR003068

Laio, F., Porporato, A., Ridolfi, L., & Rodriguez-Iturbe, I. (2001). Plants in water-controlled ecosystems: Active role in hydrologic processes and response to water stress. *Advances in Water Resources*, *24*(7), 707–723. https://doi.org/10.1016/S0309-1708(01)00005-7

Lian, X., Piao, S., Li, L. Z. X., Li, Y., Huntingford, C., Ciais, P., et al. (2020). Summer soil drying exacerbated by earlier spring greening of northern vegetation. *Science Advances*, *6*(1), eaax0255. https://doi.org/10.1126/sciadv.aax0255

Liu, L., Gudmundsson, L., Hauser, M., Qin, D., Li, S., & Seneviratne, S. I. (2020). Soil moisture dominates dryness stress on ecosystem production globally. *Nature Communications*, *11*(1), 4892. https://doi.org/10.1038/s41467-020-18631-1

Lu, L., & Shuttleworth, W. J. (2002). Incorporating NDVI-derived LAI into the climate version of RAMS and its impact on regional climate. *Journal of Hydrometeorology*, *3*(3), 347–362. https://doi.org/10.1175/1525-7541(2002)003<0347:INDLIT>2.0.CO;2

Ma, S., Baldocchi, D., Wolf, S., & Verfaillie, J. (2016). Slow ecosystem responses conditionally regulate annual carbon balance over 15 years in Californian oak-grass savanna. *Agricultural and Forest Meteorology*, *228*, 252–264. https://doi.org/10.1016/j.agrformet.2016.07.016

Ma, S., Baldocchi, D. D., Xu, L., & Hehn, T. (2007). Inter-annual variability in carbon dioxide exchange of an oak/grass savanna and open grassland in California. *Agricultural and Forest Meteorology*, *147*(3–4), 157–171. https://doi.org/10.1016/j.agrformet.2007.07.008

Mackay, D. S., Ewers, B. E., Cook, B. D., & Davis, K. J. (2007). Environmental drivers of evapotranspiration in a shrub wetland and an upland forest in northern Wisconsin. *Water Resources Research*, *43*(3), W03442. https://doi.org/10.1029/2006WR005149

Manoli, G., Domec, J., Novick, K., Oishi, A. C., Noormets, A., Marani, M., & Katul, G. (2016). Soil–plant–atmosphere conditions regulating convective cloud formation above southeastern US pine plantations. *Global Change Biology*, *22*(6), 2238–2254. https://doi.org/10.1111/gcb.13221

Markland, T. C. (2019). Carbon balance and evapotranspiration rates of a restored prairie and a conventional corn/soybean rotation.

Marvel, K., Cook, B. I., Bonfils, C., Smerdon, J. E., Williams, A. P., & Liu, H. (2021). Projected changes to hydroclimate seasonality in the continental United States. *Earth's Future*, *9*(9), e2021EF002019. https://doi.org/10.1029/2021EF002019

Matsui, T., Lakshmi, V., & Small, E. E. (2005). The effects of satellite-derived vegetation cover variability on simulated land–atmosphere interactions in the NAMS. *Journal of Climate*, *18*(1), 21–40. https://doi.org/10.1175/JCLI3254.1

Migliavacca, M., Sonnentag, O., Keenan, T. F., Cescatti, A., O'Keefe, J., & Richardson, A. D. (2012). On the uncertainty of phenological responses to climate change, and implications for a terrestrial biosphere model. *Biogeosciences*, *9*(6), 2063–2083. https://doi.org/10.5194/bg-9-2063-2012

Miralles, D. G., Teuling, A. J., van Heerwaarden, C. C., & de Arellano, J. V. G. (2014). Mega-heatwave temperatures due to combined soil desiccation and atmospheric heat accumulation. *Nature Geoscience*, *7*(5), 345–349. https://doi.org/10.1038/ngeo2141

Monteith, J. L. (1981). Evaporation and surface temperature. *Quarterly Journal of the Royal Meteorological Society*, *107*(451), 1–27. https://doi.org/10.1002/qj.49710745102

Moon, M., Li, D., Liao, W., Rigden, A. J., & Friedl, M. A. (2020). Modification of surface energy balance during springtime: The relative importance of biophysical and meteorological changes. *Agricultural and Forest Meteorology*, *284*, 107905. https://doi.org/10.1016/j.agrformet.2020.107905

Novick, K. A., Ficklin, D. L., Stoy, P. C., Williams, C. A., Bohrer, G., Oishi, A. C., et al. (2016). The increasing importance of atmospheric demand for ecosystem water and carbon fluxes. *Nature Climate Change*, *6*(11), 1023–1027. https://doi.org/10.1038/nclimate3114

Oki, T., & Kanae, S. (2006). Global hydrological cycles and world water resources. *Science*, *313*(5790), 1068–1072. https://doi.org/10.1126/science.1128845

Oren, R., Sperry, J. S., Katul, G. G., Pataki, D. E., Ewers, B. E., Phillips, N., & Schäfer, K. V. R. (1999). Survey and synthesis of intra- and interspecific variation in stomatal sensitivity to vapour pressure deficit. *Plant, Cell and Environment*, *22*(12), 1515–1526. https://doi.org/10.1046/j.1365-3040.1999.00513.x

Papale, D., Reichstein, M., Aubinet, M., Canfora, E., Bernhofer, C., Kutsch, W., et al. (2006). Towards a standardized processing of net ecosystem exchange measured with eddy covariance technique: Algorithms and uncertainty estimation. *Biogeosciences*, *3*(4), 571–583. https://doi.org/10.5194/bg-3-571-2006

Peichl, M., Arain, M. A., & Brodeur, J. J. (2010). Age effects on carbon fluxes in temperate pine forests. *Agricultural and Forest Meteorology*, *150*(7–8), 1090–1101. https://doi.org/10.1016/j.agrformet.2010.04.008

Petrie, M. D., Collins, S. L., Swann, A. M., Ford, P. L., & Litvak, M. E. (2015). Grassland to shrubland state transitions enhance carbon sequestration in the northern Chihuahuan Desert. *Global Change Biology*, *21*(3), 1226–1235. https://doi.org/10.1111/gcb.12743

Potts, D. L., Huxman, T. E., Cable, J. M., English, N. B., Ignace, D. D., Eilts, J. A., et al. (2006). Antecedent moisture and seasonal precipitation influence the response of canopy-scale carbon and water exchange to rainfall pulses in a semi-arid grassland. *New Phytologist*, *170*(4), 849–860. https://doi.org/10.1111/j.1469-8137.2006.01732.x

Puma, M. J., Koster, R. D., & Cook, B. I. (2013). Phenological versus meteorological controls on land-atmosphere water and carbon fluxes. *Journal of Geophysical Research: Biogeosciences*, *118*(1), 14–29. https://doi.org/10.1029/2012JG002088

Raz-Yaseef, N., Yakir, D., Schiller, G., & Cohen, S. (2012). Dynamics of evapotranspiration partitioning in a semi-arid forest as affected by temporal rainfall patterns. *Agricultural and Forest Meteorology*, *157*, 77–85. https://doi.org/10.1016/j.agrformet.2012.01.015

Richardson, A. D. (2019). *Tracking seasonal rhythms of plants in diverse ecosystems with digital camera imagery*. Blackwell Publishing Ltd. https://doi.org/10.1111/nph.15591

Richardson, A. D., & Hollinger, D. Y. (2005). Statistical modeling of ecosystem respiration using eddy covariance data: Maximum likelihood parameter estimation, and Monte Carlo simulation of model and parameter uncertainty, applied to three simple models. *Agricultural and Forest Meteorology*, *131*(3–4), 191–208. https://doi.org/10.1016/j.agrformet.2005.05.008

Richardson, A. D., Hufkens, K., Milliman, T., Aubrecht, D. M., Chen, M., Gray, J. M., et al. (2018). Tracking vegetation phenology across diverse North American biomes using PhenoCam imagery. *Scientific Data*, *5*(1), 180028. https://doi.org/10.1038/sdata.2018.28

Roman, D. T., Novick, K. A., Brzostek, E. R., Dragoni, D., Rahman, F., & Phillips, R. P. (2015). The role of isohydric and anisohydric species in determining ecosystem-scale response to severe drought. *Oecologia*, *179*(3), 641–654. https://doi.org/10.1007/s00442-015-3380-9

Rosseel, Y. (2012). lavaan: An R package for structural equation modeling. *Journal of Statistical Software*, *48*(2), 1–36. https://doi.org/10.18637/jss.v048.i02

Ruehr, N. K., Law, B. E., Quandt, D., & Williams, M. (2014). Effects of heat and drought on carbon and water dynamics in a regenerating semi-arid pine forest: A combined experimental and modeling approach. *Biogeosciences*, *11*(15), 4139–4156. https://doi.org/10.5194/bg-11-4139-2014

Sakai, R. K., Fitzjarrald, D. R., & Moore, K. E. (1997). Detecting leaf area and surface resistance during transition seasons. *Agricultural and Forest Meteorology*, *84*(3–4), 273–284. https://doi.org/10.1016/S0168-1923(96)02359-3

Samuels-Crow, K. E., Ogle, K., & Litvak, M. E. (2020). Atmosphere-soil interactions govern ecosystem flux sensitivity to environmental conditions in semiarid woody ecosystems over varying timescales. *Journal of Geophysical Research: Biogeosciences*, *125*(8), e2019JG005554. https://doi.org/10.1029/2019JG005554

Schär, C., Lüthi, D., Beyerle, U., & Heise, E. (1999). The soil–precipitation feedback: A process study with a regional climate model. *Journal of Climate*, *12*(3), 722–741. https://doi.org/10.1175/1520-0442(1999)012<0722:TSPFAP>2.0.CO;2

Schwartz, M. D. (1992). Phenology and springtime surface-layer change. *Monthly Weather Review*, *120*(11), 2570–2578. https://doi.org/10.1175/1520-0493(1992)120<2570:PASSLC>2.0.CO;2

Scott, R. L., & Biederman, J. A. (2017). Partitioning evapotranspiration using long-term carbon dioxide and water vapor fluxes. *Geophysical Research Letters*, *44*(13), 6833–6840. https://doi.org/10.1002/2017GL074324

Scott, R. L., Biederman, J. A., Hamerlynck, E. P., & Barron-Gafford, G. A. (2015). The carbon balance pivot point of southwestern U.S. semiarid ecosystems: Insights from the 21st century drought. *Journal of Geophysical Research: Biogeosciences*, *120*(12), 2612–2624. https://doi.org/10.1002/2015JG003181

Scott, R. L., Hamerlynck, E. P., Jenerette, G. D., Moran, M. S., & Barron-Gafford, G. A. (2010). Carbon dioxide exchange in a semidesert grassland through drought-induced vegetation change. *Journal of Geophysical Research*, *115*(G3), G03026. https://doi.org/10.1029/2010JG001348

Scott, R. L., Huxman, T. E., Cable, W. L., & Emmerich, W. E. (2006). Partitioning of evapotranspiration and its relation to carbon dioxide exchange in a Chihuahuan Desert shrubland. *Hydrological Processes*, *20*(15), 3227–3243. https://doi.org/10.1002/hyp.6329

Scott, R. L., Knowles, J. F., Nelson, J. A., Gentine, P., Li, X., Barron-Gafford, G., et al. (2021). Water availability impacts on evapotranspiration partitioning. *Agricultural and Forest Meteorology*, *297*, 108251. https://doi.org/10.1016/j.agrformet.2020.108251

Seneviratne, S. I., Corti, T., Davin, E. L., Hirschi, M., Jaeger, E. B., Lehner, I., et al. (2010). Investigating soil moisture-climate interactions in a changing climate: A review. *Earth-Science Reviews*, *99*(3–4), 125–161. https://doi.org/10.1016/j.earscirev.2010.02.004

Seyednasrollah, B., Bowling, D. R., Cheng, R., Logan, B. A., Magney, T. S., Frankenberg, C., et al. (2021). Seasonal variation in the canopy color of temperate evergreen conifer forests. *New Phytologist*, *229*(5), 2586–2600. https://doi.org/10.1111/nph.17046

Seyednasrollah, B., Young, A. M., Hufkens, K., Milliman, T., Friedl, M. A., Frolking, S. et al. (2019a). PhenoCam Dataset v2.0: Vegetation Phenology from Digital Camera Imagery, 2000-2018. ORNL Distributed Active Archive Center. https://doi.org/10.3334/ORNLDAAC/1674

Seyednasrollah, B., Young, A. M., Hufkens, K., Milliman, T., Friedl, M. A., Frolking, S., & Richardson, A. D. (2019b). Tracking vegetation phenology across diverse biomes using Version 2.0 of the PhenoCam Dataset. *Scientific Data*, *6*(1), 222. https://doi.org/10.1038/s41597-019-0229-9

Seyednasrollah, B., Young, A. M., Li, X., Milliman, T., Ault, T., Frolking, S., et al. (2020). Sensitivity of deciduous forest phenology to environmental drivers: Implications for climate change impacts across North America. *Geophysical Research Letters*, *47*(5), e2019GL086788. https://doi.org/10.1029/2019GL086788

Spinoni, J., Vogt, J., Naumann, G., Carrao, H., & Barbosa, P. (2015). Towards identifying areas at climatological risk of desertification using the Köppen-Geiger classification and FAO aridity index. *International Journal of Climatology*, *35*(9), 2210–2222. https://doi.org/10.1002/joc.4124

Stoy, P. C., Katul, G. G., Siqueira, M. B. S., Juang, J. Y., Novick, K. A., Mccarthy, H. R., et al. (2006). Separating the effects of climate and vegetation on evapotranspiration along a successional chronosequence in the southeastern US. *Global Change Biology*, *12*(11), 2115–2135. https://doi.org/10.1111/j.1365-2486.2006.01244.x

Thomas, C. K., Law, B. E., Irvine, J., Martin, J. G., Pettijohn, J. C., & Davis, K. J. (2009). Seasonal hydrology explains interannual and seasonal variation in carbon and water exchange in a semiarid mature ponderosa pine forest in central Oregon. *Journal of Geophysical Research*, *114*(G4), G04006. https://doi.org/10.1029/2009JG001010

Thompson, S. E., Harman, C. J., Konings, A. G., Sivapalan, M., Neal, A., & Troch, P. A. (2011). Comparative hydrology across AmeriFlux sites: The variable roles of climate, vegetation, and groundwater. *Water Resources Research*, *47*(10), W00J07. https://doi.org/10.1029/2010WR009797

Trabucco, A., & Zomer, R. (2019). Global aridity index and potential evapotranspiration (ET0) climate database v2. [Dataset]. Figshare. https://doi.org/10.6084/Fm9.figshare.7504448

Tyree, M. T., & Ewers, F. W. (1991). The hydraulic architecture of trees and other woody plants. *New Phytologist*, *119*(3), 345–360. https://doi.org/10.1111/j.1469-8137.1991.tb00035.x

Villegas, J. C., Breshears, D. D., Zou, C. B., & Law, D. J. (2010). Ecohydrological controls of soil evaporation in deciduous drylands: How the hierarchical effects of litter, patch and vegetation mosaic cover interact with phenology and season. *Journal of Arid Environments*, *74*(5), 595–602. https://doi.org/10.1016/j.jaridenv.2009.09.028

Vivoni, E. R., Moreno, H. A., Mascaro, G., Rodriguez, J. C., Watts, C. J., Garatuza-Payan, J., & Scott, R. L. (2008). Observed relation between evapotranspiration and soil moisture in the North American monsoon region. *Geophysical Research Letters*, *35*(22), L22403. https://doi.org/10.1029/2008GL036001

Wang, L., Good, S. P., & Caylor, K. K. (2014). Global synthesis of vegetation control on evapotranspiration partitioning. *Geophysical Research Letters*, *41*(19), 6753–6757. https://doi.org/10.1002/2014GL061439

Williams, C. A., Reichstein, M., Buchmann, N., Baldocchi, D., Beer, C., Schwalm, C., et al. (2012). Climate and vegetation controls on the surface water balance: Synthesis of evapotranspiration measured across a global network of flux towers. *Water Resources Research*, *48*(6), W06523. https://doi.org/10.1029/2011WR011586

Williams, I. N., & Torn, M. S. (2015). Vegetation controls on surface heat flux partitioning, and land-atmosphere coupling. *Geophysical Research Letters*, *42*(21), 9416–9424. https://doi.org/10.1002/2015GL066305

Wilson, K. B., & Baldocchi, D. D. (2000). Seasonal and interannual variability of energy fluxes over a broadleaved temperate deciduous forest in North America. *Agricultural and Forest Meteorology*, *100*(1), 1–18. https://doi.org/10.1016/S0168-1923(99)00088-X

Wilson, K. B., Hanson, P. J., & Baldocchi, D. D. (2000). Factors controlling evaporation and energy partitioning beneath a deciduous forest over an annual cycle. *Agricultural and Forest Meteorology*, *102*(2–3), 83–103. https://doi.org/10.1016/S0168-1923(00)00124-6

Wolf, S., Keenan, T. F., Fisher, J. B., Baldocchi, D. D., Desai, A. R., Richardson, A. D., et al. (2016). Warm spring reduced carbon cycle impact of the 2012 US summer drought. *Proceedings of the National Academy of Sciences of the United States of America*, *113*(21), 5880–5885. https://doi.org/10.1073/pnas.1519620113

Yan, D., Scott, R. L., Moore, D. J. P., Biederman, J. A., & Smith, W. K. (2019). Understanding the relationship between vegetation greenness and productivity across dryland ecosystems through the integration of PhenoCam, satellite, and eddy covariance data. *Remote Sensing of Environment*, *223*, 50–62. https://doi.org/10.1016/j.rse.2018.12.029

Yao, J., Liu, H., Huang, J., Gao, Z., Wang, G., Li, D., et al. (2020). Accelerated dryland expansion regulates future variability in dryland gross primary production. *Nature Communications*, *11*(1), 1665. https://doi.org/10.1038/s41467-020-15515-2

Zavaleta, E. S., Thomas, B. D., Chiariello, N. R., Asner, G. P., Shaw, M. R., & Field, C. B. (2003). Plants reverse warming effect on ecosystem water balance. *Proceedings of the National Academy of Sciences*, *100*(17), 9892–9893. https://doi.org/10.1073/pnas.1732012100

Zhang, L., Dawes, W. R., & Walker, G. R. (2001). Response of mean annual evapotranspiration to vegetation changes at catchment scale. *Water Resources Research*, *37*(3), 701–708. https://doi.org/10.1029/2000WR900325

References From the Supporting Information

Richardson, A. D., Hollinger, D. Y., Shoemaker, J., Hughes, H., Savage, K., & Davidson, E. A. (2019). Tower- and chamber-based greenhouse gas flux measurements from Howland Forest, Maine (2012–2018) [Dataset]. figshare. https://doi.org/10.6084/m9.figshare.7445657.v1

Richardson, A. D., Hollinger, D. Y., Shoemaker, J. K., Hughes, H., Savage, K., & Davidson, E. A. (2019). Six years of ecosystem-atmosphere greenhouse gas fluxes measured in a sub-boreal forest. *Scientific Data*, *6*(1), 117. https://doi.org/10.1038/s41597-019-0119-1